frontiers in Earth Science

BRIEF RESEARCH REPORT
published: 03 February 2022
doi: 10.3389/feart.2022.799097

New Discovery of Oligocene Strata in the Topernawi Formation, Turkana County, Kenya

Francis J. Sousa[1], Stephen E. Cox[2], Sidney R. Hemming[2], E. Troy Rasbury[3], Elena Steponaitis[4], Kevin Hatton[3], Mae Saslaw[3], Gregory Henkes[3], Patricia Princehouse[5], Natasha S. Vitek[6] and Isaiah Nengo[7]*

[1]College of Earth, Ocean, and Atmospheric Sciences, Oregon State University, Corvallis, OR, United States, [2]Lamont-Doherty Earth Observatory, Columbia University, Palisades, NY, United States, [3]Department of Geosciences, Stony Brook University, Stony Brook, NY, United States, [4]Department of Earth and Environmental Sciences, Tulane University, New Orleans, LA, United States, [5]Institute for the Science of Origins, Case Western Reserve University, Cleveland, OH, United States, [6]Department of Ecology and Evolution, Stony Brook University, Stony Brook, NY, United States, [7]Turkana Basin Institute, Stony Brook University, Stony Brook, NY, United States

New field observations and $^{40}Ar/^{39}Ar$ geochronology reveal that the Topernawi Formation of the Ekitale Basin, northern Turkana Depression, Turkana County, Kenya was deposited entirely during the Oligocene between 29.7 ± 0.5 Ma and 29.24 ± 0.08 Ma. These bracketing ages are determined via new $^{40}Ar/^{39}Ar$ geochronology on a basaltic lava flow at the base of the section and a felsic ignimbrite near the top. A newly discovered basal unit and interbedded lava flow result in a new total sedimentary thickness of 92 m. The Topernawi Formation is the oldest dated syn-rift sedimentary section in the northern Turkana Depression.

Keywords: East Africa rift system, oligocene, hominid evolution, stratigraphy, geochronology, Turkana basin, Turkana depression

OPEN ACCESS

Edited by:
Laura Christine Gregory, University of Leeds, United Kingdom

Reviewed by:
Christopher Keith Morley, PTT Public Company Limited, Thailand
Samuel C. Boone, The University of Melbourne, Australia

****Correspondence:***
Francis J. Sousa
francis.sousa@oregonstate.edu

Specialty section:
This article was submitted to Structural Geology and Tectonics, a section of the journal Frontiers in Earth Science

Received: *21 October 2021*
Accepted: *04 January 2022*
Published: *03 February 2022*

Citation:
Sousa FJ, Cox SE, Hemming SR, Rasbury ET, Steponaitis E, Hatton K, Saslaw M, Henkes G, Princehouse P, Vitek NS and Nengo I (2022) New Discovery of Oligocene Strata in the Topernawi Formation, Turkana County, Kenya. Front. Earth Sci. 10:799097. doi: 10.3389/feart.2022.799097

1 INTRODUCTION

The East African Rift System (EARS) is an active continental rift that initiated during Paleogene time (Morley et al., 1992; Morley et al., 1999; Vétel et al., 2005; Vetel and Le Gall, 2006) and hosts numerous sedimentary sections that have played a key role in recording hominid evolution (Coffing et al., 1994; Leakey et al., 2001; Ducrocq et al., 2010; Roberts et al., 2012). Additionally the EARS has played an integral role in the development of conceptual and analog models for the succession of rift stages from pre-inception through maturity (Cowie et al., 2000). Despite it being one of the type examples of continental rifting, the initiation and early history of the EARS is poorly known (Boone et al., 2019). As with many complex Earth systems, the initial crustal conditions of continental rifting are important factors controlling the geometry and location of rift development (e.g., through re-activation of pre-existing structures). In the case of the EARS, these initial conditions are characterized by the geometry, structure, and spatio-temporal evolution of the pre-EARS lithosphere. In northern Kenya, the EARS cuts across a Mesozoic rift system called the Central African Rift System [CARS; **Figure 1**; (Ebinger et al., 2000; Vétel et al., 2005; Macgregor, 2015; Boone et al., 2018)]. Although there is significant direct evidence for the pre-EARS condition in the Turkana Depression, it is difficult to fully characterize the pre-EARS lithospheric structure. It is notable that the spatial extent of regionally lower elevations known as the Turkana Depression is roughly coincident with the overlap of the CARS and EARS (**Figure 1**).

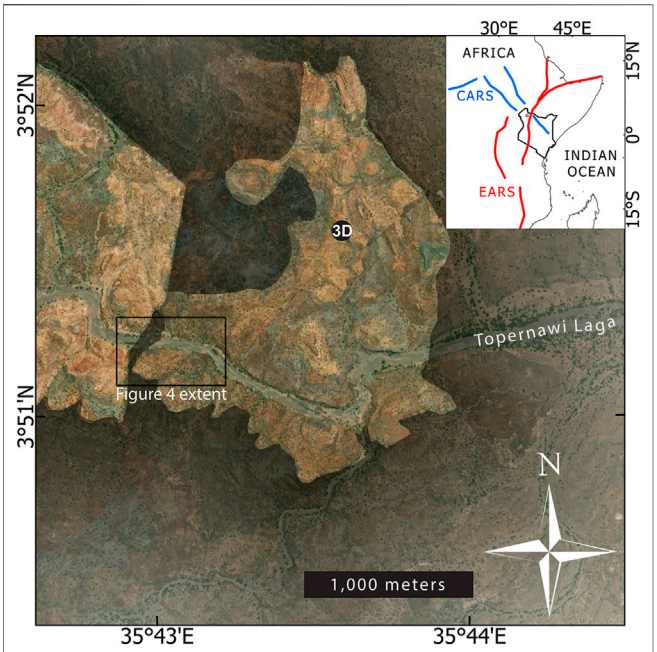

FIGURE 1 | Satellite imagery of the study area. Boundary of the Topernawi Formation is delineated by gray shading. Label "3D" shows location of the field photo in **Figure 3D**. Box outlined in thin black line shows extent of **Figure 4**. Inset map shows outline of Africa (thin black line), Kenya (thick black line), and generalized structure of the EARS (red) and CARS (blue) after (Macgregor, 2015). Extent of main frame is shown as very small box on inset map.

The Turkana Depression hosts a diversity of sedimentary rocks, including Cretaceous-Paleogene sediments that mostly pre-date EARS inception (e.g., Lapur Formation) and a wide variety of richly fossiliferous Miocene and younger syn-rift sedimentary rocks [e.g., Lothidok Formation, Koobi Fora Formation, Galanaboi Formation; (Ragon et al., 2019; Morley, 2020) and citations therein]. The timing of local onset of EARS extension in the Turkana Depression is recorded in well and outcrop data by the Eocene-Oligocene sedimentary record of the Lokichar Basin (Morley et al., 1992; Morley et al., 1999; Boone et al., 2019), Eocene-Oligocene faulting east of Lake Turkana (Vetel and Le Gall, 2006), Oligocene growth of North Lokichar Basin, North Kerio Basin, and southern Turkana Basin (Morley et al., 1999; Morley, 1999b; Boone et al., 2018; Schofield et al., 2021) and two approximately north-south trending subsurface basins of possible Paleogene age (Wescott et al., 1999). Elsewhere in Turkana, EARS onset is primarily marked by widespread mafic volcanism [Asile Group: circa 34.3–15 Ma (McDougall and Watkins, 2006), Turkana Volcanics Formation: circa 38–29.7 Ma (McDougall and Brown, 2009; Ragon et al., 2019), Kalokol Formation: circa 28–18.5 Ma (Boschetto et al., 1992)]. Because so much of the Turkana Depression rock record from the early phase of EARS evolution is dominated by mafic volcanics, the sedimentary rocks and the paleoenvironmental, palaeoecological, and paleontological data they hold are extremely limited.

The Topernawi Formation of the Ekitale Basin, Turkana County, Kenya, contains syn-extensional Oligocene sedimentary and felsic volcanic rocks deposited during this early phase of the EARS (Ragon et al., 2019). Other known sedimentary rocks of this age are limited to the southern part of the Turkana Depression—the Lokhone Formation in the Lokichar Basin (Morley et al., 1999; Ducrocq et al., 2010). Accordingly, the Topernawi Formation is uniquely positioned to provide crucial evidence for understanding the Oligocene geologic and landscape evolution of the northern Turkana Depression. The fossiliferous parts of the Topernawi Formation contain rich floral and faunal assemblages that provide critical evidence for the paleoecology and paleoclimate of the Paleogene, an important time period in mammal evolution (Werdelin and Sanders, 2010; Jaeger et al., 2019).

The extent of the Topernawi Formation was first described with a geologic map at approximately 1:50,000 scale based on field observations, remote sensing data, a local stratigraphy composed of 75 m of measured section (Ragon et al., 2019; Sousa et al., 2020), and several $^{40}Ar/^{39}Ar$ ages from volcanic rocks outcropping in the area (McDougall and Brown, 2009; Ragon et al., 2019). Ragon et al. (2019) used these observations to interpret a detailed polyphase paleoenvironmental and regional tectono-morphic evolution that integrated the stratigraphic and chronologic data into a coherent basin-scale and regional framework. The purpose of this paper is to build upon the understanding developed in Ragon et al. (2019) by presenting new field observations and geochronology that significantly refine the timing and rate of Topernawi Formation deposition and frame the exciting potential of this site for future work to understand Oligocene tectonics, paleontology, and paleoecology.

2 METHODS

2.1 Field Work

This study involved eight field days over two seasons in the vicinity of Topernawi Laga, Turkana County, Kenya. All logistics were coordinated through the Turkana Basin Institute, Turkwel Camp. Field data was collected digitally and by hand. Handheld Garmin GPSMap® units were utilized to track and record locations. Geologic mapping was completed on mylar over a satellite imagery base at 1:5,000 scale. Field sheets were digitized in ESRI ArcGIS Pro. Of the rock samples collected in the field, two were used for radiometric dating as described in the next section.

2.2 Analytical Methods

Both samples were processed at the Stony Brook University FIRST lab. The basalt sample 20TB23 was crushed, sieved to 300–500 μm, and hand-picked to isolate clean, fine-grained basalt groundmass with no visible mineral crystals. The ignimbrite sample 20TB20 was crushed and sieved to 125–250 μm, then sodium polytungstate was used to isolate the $2.55>\rho>2.65$ fraction, which was then hand-picked to isolate clean feldspar crystals with no visible inclusions. Both samples were co-irradiated at the Oregon State TRIGA Reactor

with the Fish Canyon Tuff sanidine monitor standard. The samples and standards were loaded together in adjacent pits at the same depth in a 1.9 cm diameter, 0.3 cm depth Al disk (Renne et al., 1998). Sample 20TB20 was irradiated for 14 h (J = 3.785e-3 ± 4.2e-6), and sample 20TB23 was irradiated for 8 h (J = 2.126e-3 ± 2.2e-6). Stacked disks were wrapped in Al foil and placed in a cadmium-shielded irradiation tube at the TRIGA facility. The true $^{40}Ar/^{36}Ar$ ratio of air was assumed to be 298.56 as reported by Lee et al. (2006). The $^{40}Ar/^{39}Ar$ ratios for age determination were then calculated using the nuclear interference corrections of Renne et al. (1998) and a J value calculated using the age of 28.201 ± 0.046 Ma for the Fish Canyon Tuff sanidine monitor standard (28.201 ± 0.046 Ma, Kuiper et al., 2008), using decay constants of Min et al. (2000). We report the uncertainty of the age determination of each sample at two standard deviations to provide better confidence in comparison with other methodologies and the absolute geologic timescale.

Sample 20TB23 was wrapped in a Ta tube, placed in a Cu sample holder, and heated sequentially over 14 steps with a Photon Machines Fusions diode laser (970 nm wavelength). Each of 14 steps lasted 600 s with heating power ranging from 0.075 to 24 W. Gases evolved were exposed to two hot (~400°C) SAES St 101 Zr-Al non-evaporable getter for 11 min. Purified Ar was released from the getter chamber into a VG 5400 mass spectrometer for 60 s, during which time the 40Ar signal was monitored. The VG 5400 was set to 4500 V accelerating voltage and 200 μA trap current and tuned for good sensitivity and best isotope ratio linearity. Samples were measured with calibrated air standards and procedural blanks to account for mass discrimination and instrument backgrounds, and all five Ar isotopes (^{36}Ar, ^{37}Ar, ^{38}Ar, ^{39}Ar, ^{40}Ar) were measured sequentially in peak-hopping mode on the analog multiplier. Plateau ages were defined as three or more contiguous steps corresponding to a minimum of 50% of the 39Ar released and showing no statistically significant slope. Reported ages are corrected for trapped Ar with the isotopic composition of air, which is indistinguishable from the apparent trapped initial calculated from placing all steps on an isochron. Steps 9–12 produced a plateau with an age of 29.7 ± 0.5 Ma (2σ SE; **Supplemental Material**) representing 69.5% of the 39Ar in the sample.

Twenty crystals from sample 20TB20 were isolated and placed in a Ti sample holder, then individually heated to fusion using an 8.4 W, 45-s heating with a Photon Machines Fusions CO2 laser with the lens positioned to provide a ~3 mm beam. Gases evolved were exposed to a hot (~400°C) SAES St 101 Zr-Al non-evaporable getter for 5 min. Purified Ar was released from the getter chamber into the Isotopx NGX-600 mass spectrometer for 30 s, during which time the signal was monitored on all detectors. The Isotopx NGX-600 multicollector mass spectrometer was set to 6000 V accelerating voltage and 200 μA trap current and tuned for good sensitivity and best isotope ratio linearity. Samples were measured with calibrated air standards and procedural blanks to account for mass discrimination and instrument backgrounds, and all five Ar isotopes (36, 37, 38, 39, 40Ar) were measured simultaneously, with the 36Ar measured on an ion-counting multiplier and the rest measured on Faraday collectors equipped with ATONA amplifiers (Cox et al., 2020). One crystal produced blank-level Ar and is presumed to be a different mineral. The remaining 19 crystals produced ages ranging from 28.57 ± 0.13 to 30.47 ± 0.34 Ma (1σ). We rejected the single young outlier due to anomalously low radiogenic Ar fraction (31.5%) and the three older outliers due to the fact that older outliers in an ignimbrite likely represent detrital material from previous eruptions. The remaining 15/19 analyses produced a single age population with a weighted mean age of 29.24 ± 0.08 Ma (2σ; **Supplemental Material**).

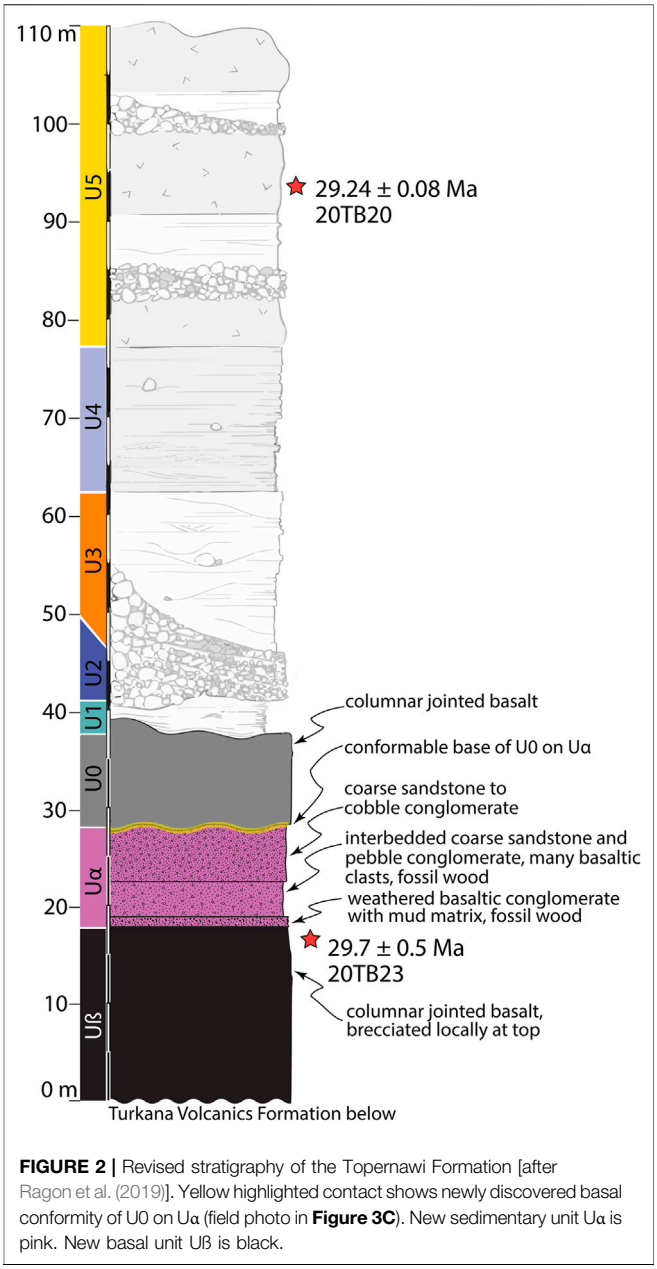

FIGURE 2 | Revised stratigraphy of the Topernawi Formation [after Ragon et al. (2019)]. Yellow highlighted contact shows newly discovered basal conformity of U0 on Uα (field photo in **Figure 3C**). New sedimentary unit Uα is pink. New basal unit Uß is black.

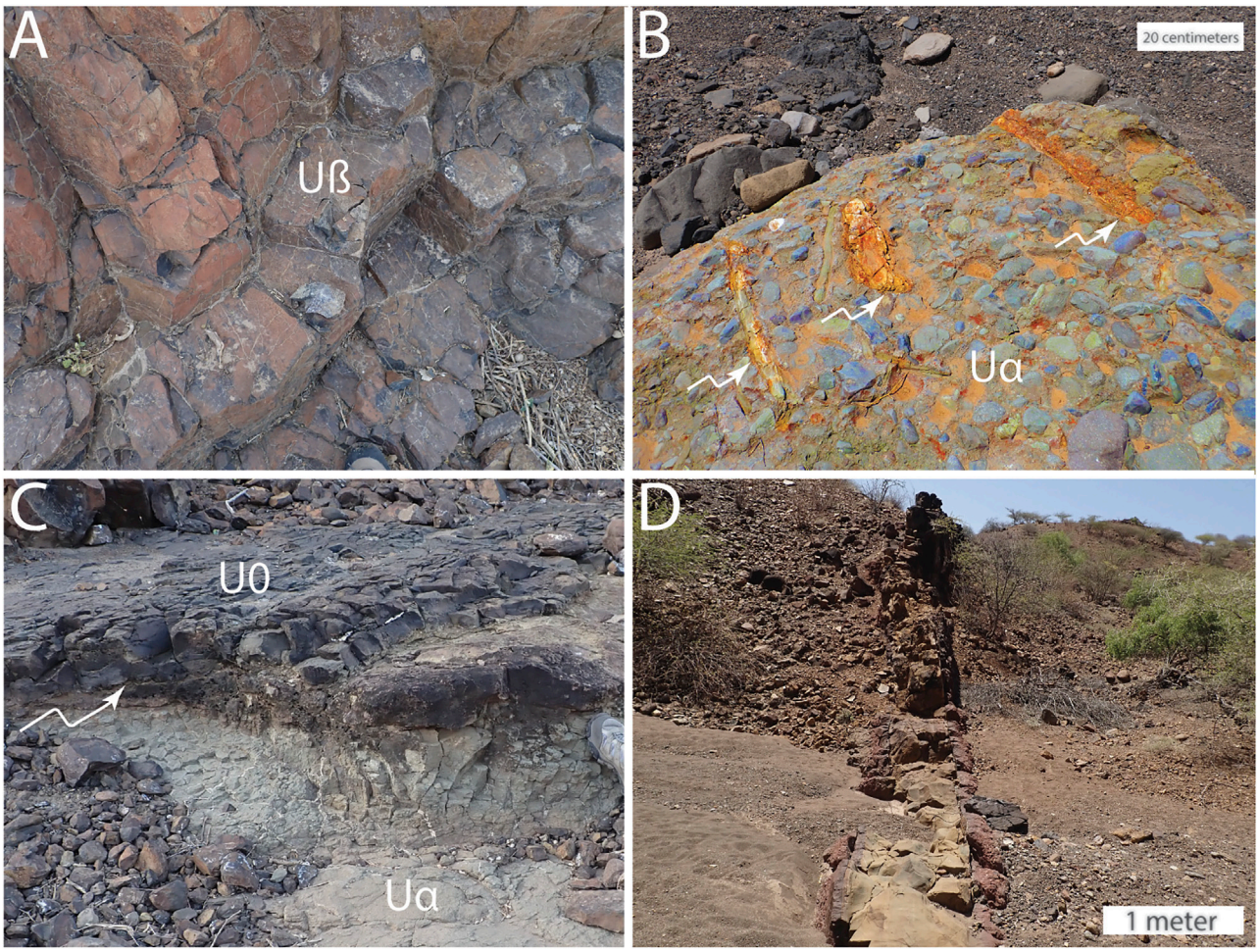

FIGURE 3 | Four field photos from the study area. **(A)** Columnar jointed basalt of new basal unit Uß (20TB23). Toe box of boot for scale at bottom of image. Location: 3.853661°N, 35.715842°E. **(B)** Conglomerate in unit Uα. Clasts are predominantly of weathered mafic volcaniclastic composition. White arrows point to chunks of fossil wood. Colors are enhanced to increase visibility of clasts and contrast with alluvium in background. Location: 3.853731°N, 35.718022°E. **(C)** New discovery of conformable base of unit U0 on unit Uα. White arrow points to conformable contact. Toe box of boot for scale at right side of image. Location: 3.853398°N, 35.719134°E. For detailed location of photos in **(A–C)**, **Figure 4** caption. **(D)** Mafic dike cutting through Topernawi Formation. Location shown on **Figure 1** (3.860148°N, 35.725909°E).

3 RESULTS

3.1 Revised Stratigraphy and New Geochronology

We report here 22 m of new section at the base of the Topernawi Formation. We broadly adopt the stratigraphic nomenclature of Ragon et al. (2019) and accommodate the newly discovered section by adding two new basal units (Uα and Uß; **Figure 2**). No names of previously described units are changed. We also report data from two samples of the Topernawi Formation, one at the base of the section and one in the uppermost unit. Together these data constrain the depositional age of the Topernawi Formation.

3.1.1 Unit Uß

Uß is a columnar jointed basalt (**Figure 3A**) that is locally brecciated in the upper meter near the depositional contact with the overlying unit Uα. The base of Uß is not exposed, so its outcrop thickness of 18 m is a minimum estimate. Uß is the lowest stratigraphic unit exposed in outcrop along the Topernawi Laga in the study area. Whole rock $^{40}Ar/^{39}Ar$ geochronology from a sample of this unit yielded an age of 29.7 ± 0.5 Ma (2σ) (20TB23; IGSN: IEFS30002; **Supplemental Material**).

3.1.2 Unit Uα

Unit Uα consists of 10 m of section exposed along Topernawi Laga in the vicinity of 3.853381° N, 35.718936° E. At the base is 1–2 m of weathered mafic volcaniclastic conglomerate with mud matrix and common decimeter-scale fossil wood chunks. The upper 8–9 m of section comprise 1 to 3-m-thick beds of coarse sandstone to cobble conglomerate and pebble conglomerate, with predominantly mafic volcaniclastic composition and common fossil wood (**Figure 3B**). We

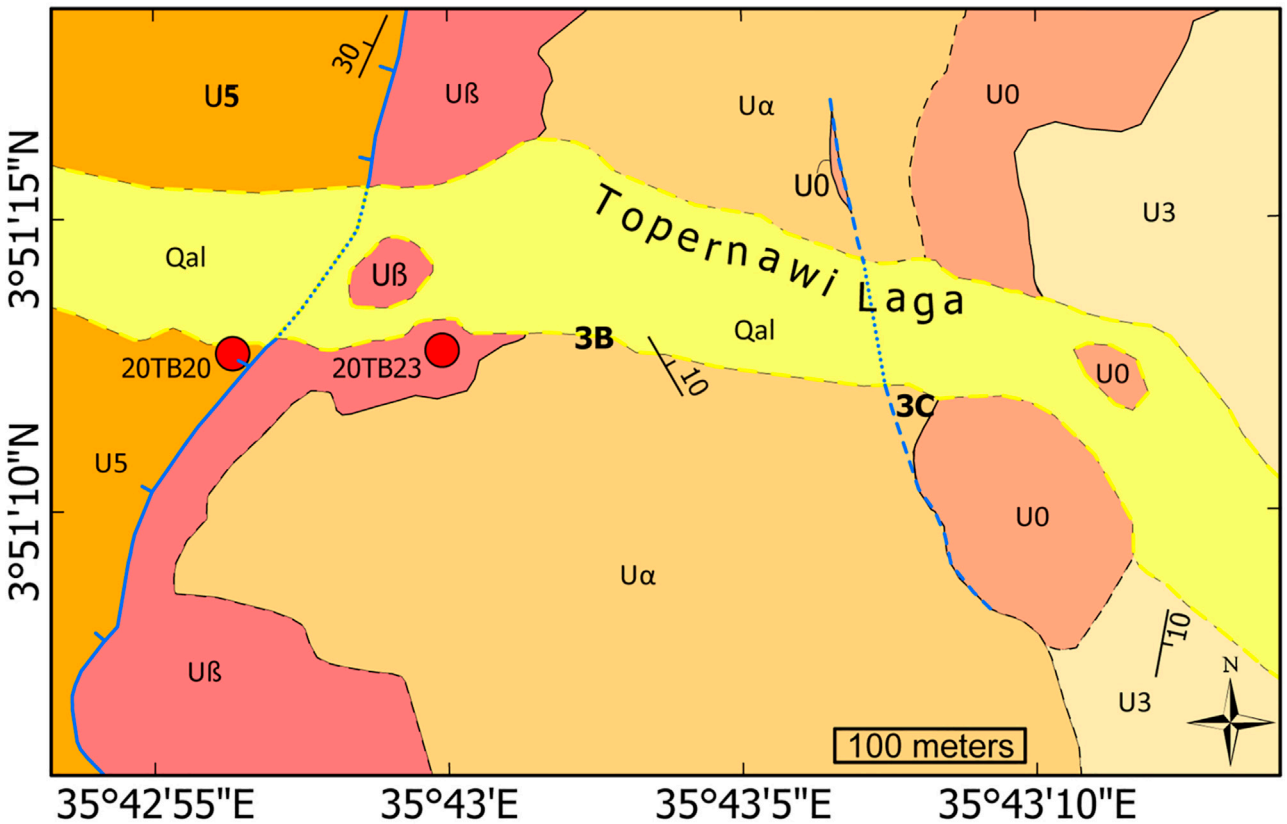

FIGURE 4 | Geologic map of the portion of the Topernawi Formation where the newly discovered units outcrop and new geochronology samples were taken (extent shown on **Figure 1**). Qal is Quaternary alluvium of Topernawi Laga. Contacts are shown as solid where well located, dashed where approximated, dotted where concealed. Faults are in blue, depositional contacts are in black. Bedding attitude measurements are shown as strike and dip symbol with dip angle adjacent to symbol. Large red circles show location of new geochronology samples. Location of photo in **Figure 3A** is at 20TB23. Location of photo in **Figure 3B** is labeled in black lettering as 3B. Location of photo is **Figure 3C** is shown in black lettering as 3C.

interpret unit Uα as the basal sedimentary deposits of the Topernawi Formation, likely representative of the initial phase of deposition of the Topernawi Formation and sourced from the locally derived weathered top of the underlying Uß unit.

3.1.3 Unit U0

Unit U0 was previously defined as the base of the Topernawi Formation by Ragon et al. (2019), and so it was not previously assigned a thickness. Newly discovered field relations clearly indicate that this unit has a conformable base where it overlies unit Uα (**Figure 3C**). This discovery redefines unit U0 as an interbedded lava flow and allows for a measure of its thickness of 12 m.

3.1.4 Unit U5

Unit U5 has been described as alternating pyroclastic, fluvial, and alluvial deposits (Ragon et al., 2019). It is most notably punctuated by up to decameter thick felsic ignimbrites deposited as pyroclastic flows. We report a new emplacement age of 29.24 ± 0.08 Ma (2σ), based on $^{40}Ar/^{39}Ar$ dating of feldspars separated from the thickest of the U5 ignimbrites at 3.853762°N, 35.71464°E (20TB20; IGSN: IEFS30001; **Supplemental Material**).

Geologic Mapping

New geologic mapping presented here is limited to the area where the basal units were discovered and new geochronologic samples were taken (**Figure 4**). All of our new data are shown on the map, including the location of the conformable base of U0 where it rests on Uα (field photo shown in **Figure 3C**), and the locations of the geochronology samples from Uß (20TB23) and U5 (20TB20). East of the major normal fault in the western portion of the map area, bedding attitudes dip gently to the east (around 10°). West of the normal fault, bedding dips more steeply and to the west, likely related to local fault-related deformation. A minor fault crosses Topernawi Laga just west of the U0/Uα contact, resulting in a repetition of section on the north flank of the Laga. Field relations do not allow for a precise measurement of the magnitude or orientation of offset on this minor structure, but it is likely limited to at most a few meters. This structure does not obfuscate the well-exposed base of U0 where it conformably overlies Uα (**Figure 3C**, location shown on **Figure 4**).

4 DISCUSSION

The Topernawi Formation of the Ekitale Basin provides a sedimentological snapshot of an Oligocene phase of early EARS evolution during which much of the Turkana Depression is dominated by mafic volcanism—the Turkana Volcanics Formation, Kalakol ß, and Asile Group (Boschetto et al., 1992; Morley, 1999a; McDougall and Watkins, 2006). Despite significant subsurface data indicating that extension was likely widespread across the northern Turkana Depression [e.g., (Morley et al., 1999; Wescott et al., 1999; Schofield et al., 2021)], to the best of our knowledge, the Topernawi Formation is the only directly dated sedimentary section of this age in the northern Turkana Depression. The only other dated sedimentary section that outcrops in the Turkana Depression and is known to span this time is the Lokhone Formation and underlying Loperot Shale of the Lokichar Basin, in the southern part of the Turkana Depression (Morley et al., 1999; Hautot et al., 2000; Muia, 2015; Ragon et al., 2019; Morley, 2020). The work presented here builds upon the foundation of Ragon et al. (2019), who documented the extent of the Topernawi Formation, used sedimentology to reconstruct depositional environments, and placed the section in a regional tectonic framework. Ragon et al. (2019) interpret the Topernawi Formation as a syn-rift package based primarily on sedimentological observations (alluvial fan deltas) and the contemporaneous relationship between the basin bounding geologic structures (normal faults) and sedimentary deposits. Our new stratigraphic and chronologic data significantly improve the constraints on the age and duration of deposition. These new constraints help refine models for the early EARS evolution and serve as a solid foundation for future multidisciplinary studies of early EARS deposits in the Turkana Depression.

4.1 Depositional Age and Estimated Accumulation Rate

Our new data constrain the depositional age of the Topernawi Formation. The age of the stratigraphically lowest unit (Uß) is 29.7 ± 0.5 Ma (2σ). The age of an ignimbrite in Unit U5 near the top of the section is 29.24 ± 0.08 Ma (2σ). This indicates that the entire section was deposited circa 30 to 29.2 Ma, which we adopt as the preferred depositional age for the entirety of the Topernawi Formation section.

Utilizing the uncertainty estimate of 0.5 million years (2σ) on the whole rock $^{40}Ar/^{39}Ar$ age from the basal lava flow, we can also calculate a rough estimate of the minimum long-term average accumulation rate for the 92 m of total section. Using 30.2 Ma as an upper bound on the age of unit Uß, we calculate a minimum average accumulation rate of 90 m per million years. This estimate is a low value relative to other published average sediment accumulation rates in continental depositional environments (Sadler, 1981; Sadler, 1999). It is likely that this minimum bound for the mean accumulation rate over the lifespan of the basin significantly underestimates the true sediment accumulation rate for the Topernawi Formation.

4.2 Published Geochronology

Previous workers have estimated the depositional age of the Topernawi Formation based on $^{40}Ar/^{39}Ar$ and K/Ar dates. While none of these previous data include samples from the upper part of the section, it is worth summarizing here the previously published data to clarify how our new data supersede them. The first date from the vicinity of Topernawi Laga was reported by McDougal and Brown. (2009) as a basalt whole rock K/Ar age of 27.9 ± 0.3 Ma (sample 98–314 therein). The sample is described as "interbedded with palagonitic breccia and clastic sediments about 1.1 km west of where Topernawi Laga enters the western margin of the Turkana Basin" and the location of 3.854°N, 35.720°E is listed. This GPS point is in the general vicinity of the U0/Uα contact (**Figure 4**), but it is not located in Topernawi Laga. The date is generally suspect as the precise location is not possible to ascertain, and the K/Ar method used is antiquated for use with whole rock basalt samples.

In addition, Ragon et al. (2019) published four new $^{40}Ar/^{39}Ar$ dates from mafic igneous rocks taken from the study area. One of those is from a basaltic lava flow described as the top of Turkana Volcanics Formation, which is interpreted by Ragon et al. (2019) to be the base of the Topernawi Formation—unit U0. Unfortunately, the GPS coordinate listed in the data table of Ragon et al. (2019) was not the true location sampled, nor did it match the location of the sample marker shown on **Figure 3B** therein. We believe that the correct location for sample 1 of Ragon et al. (2019) is 3.8541369°N, 35.719835°E (T. Ragon, written communication). Because of the proximity of the sample to our newly discovered basal section, the location of the samples is very important to precisely understanding the chronology. Due to the confusion surrounding the location, we prefer to use our new geochronology for the interpretations presented in this work. It is also worth noting that the precision of the feldspar date of sample 20TB20 is significantly higher than any of the other dates from the Topernawi Formation. Based on this date, our preferred depositional age for the entirety of the Topernawi Formation section is circa 30 to 29.2 Ma.

The other three dates published in Ragon et al. (2019) are from mafic dikes that crosscut the section in multiple locations around the study area, ranging in age from 13.9 to 25 Ma (e.g., field photo show in **Figure 3D**). While the chronology and orientation of the dikes is important for interpreting the detailed structural evolution and geometry of the basin, they are superseded as constraints on the depositional age of the Topernawi Formation by the new age from unit U5 (20TB20).

4.3 Implications for EARS Rift Evolution

The earliest stages of EARS evolution remain poorly understood [e.g., Boone et al. (2019)]. Geologic evidence for the spatio-temporal regional tectonic evolution that characterizes EARS initiation consists of seismic and well data (Morley et al., 1992; Morley et al., 1999; Morley, 1999b; Wescott et al., 1999; Schofield et al., 2021), emplacement ages and spatial patterns of mafic volcanic rocks (Morley C., 1999), and basement and detrital thermochronology (Boone et al., 2018; Boone et al., 2019). While it is unfortunate that in the northern Turkana Depression the seismic data lacks direct geologic constraints, these studies do

provide significant seismic evidence suggesting that similar aged and possibly older syn-rift strata may be preserved at depth in numerous basins in the northern Turkana Depression. Additionally, the low temperature thermochronology data is interpreted as recording short wavelength footwall uplift related to Paleogene basin formation (Boone et al., 2018). Together these lines of evidence support the interpretation of a Paleogene initiation of processes that mark the inception of true continental rifting—extensional tectonics, sedimentary accumulation, and volcanism—as opposed to pre-rift mantle plume related processes—volcanism, uplift, exhumation—that may have been genetically related to the African superswell (Gurnis et al., 2000; Moucha and Forte, 2011). In this context, the Topernawi Formation of the Ekitale Basin records the earliest dated syn-rift EARS sedimentary accumulation in outcrop at circa 29.7 to 29.2 Ma, provides a directly observable analog for the seismically imaged Paleogene basins, and adds a new datapoint to the rare evidence of Paleogene felsic volcanism in the Turkana Depression (Brown and Mcdougall, 2011).

4.4 The Western Basin

A few kilometers west of the Topernawi Formation outcrops, Ragon et al. (2019) identified a second previously unknown basin, which they refer to as the "western basin". Ragon et al. (2019) note that access to the vicinity of the western basin is difficult, and data was limited to a single paleocurrent measurement. The lack of lithologic, sedimentologic, and structural data from the western basin leaves wide-open the question of its provenance and relationship to the Topernawi Formation. Whether the strata of the western basin are time-equivalent and lithologically similar to the Topernawi Formation, or of a unique age and provenance, it holds great potential as an additional early EARS sedimentary section from the northern Turkana Depression. The western basin is currently a target for future field work, and strategies for improving access are under development.

5 CONCLUSION

A newly discovered basal unit of the Topernawi Formation (Uα) now results in a total section thickness of 92 m, including an interbedded lava flow in the lower part of the section (unit U0). Two new $^{40}Ar/^{39}Ar$ dates from a subjacent lava flow that makes up the base of the section (unit Uß) and an ignimbrite in the uppermost unit (U5), constrain the depositional age of the Topernawi Formation to be circa 30 to 29.2 Ma. This new chronology makes the Topernawi Formation the oldest dated syn-rift sedimentary section in the northern Turkana Depression, providing key evidence for the early phases of EARS evolution.

DATA AVAILABILITY STATEMENT

The Ar geochronology data generated for this study can be found in the EarthChem database (http://doi.org/10.26022/IEDA/112160). Sample 20TB20 is registered in SESAR under ISGN IEFS30001. Sample 20TB23 is registered in SESAR under ISGN IEFS30002.

AUTHOR CONTRIBUTIONS

FS led project conceptualization, field data collection and new field observations, created all figures, and wrote and edited the manuscript. All co-authors contributed to manuscript editing. SC and SH completed Ar geochronology analyses. KH and ER participated in one field season and sample preparation for Ar analyses. ES and MS participated in one field season. GH facilitated the first field season. PP co-directed the second field season. NV co-directed the second field season and participated in geologic mapping during the second field season. IN facilitated all field logistics.

FUNDING

The first field season was funded by a grant from the Turkana Basin Institute Research Fund to GH. The second field season was funded through a grant from the Turkana Basin Institute Research Fund to PP. Geochronology analyses were funded by NSF EAR award number 202166 to SH and SC, and NSF EAR award number 2021579 to ER. Partial funding for FS was provided through NSF BCS award number 2124791 to FS. Additional travel support was provided by the Columbia University Global Centers President's Global Innovation Fund. Funding for three African students to participate in the second field season was from a Leakey Foundation grant to IN. Open access publication charge was funded by a grant from the Turkana Basin Institute Research Fund to FS.

ACKNOWLEDGMENTS

We are deeply appreciative for the field logistics and personnel support of the Turkana Basin Institute, Turkwel Field Station, especially from Francis Ekai Emekwi and John Ekusi. We also thank Christopher Morley, Samuel Boone, and associate editor Laura Gregory whose reviews significantly improved this manuscript. We thank the National Museums of Kenya, the Turkana County Government, and the Government of Kenya for granting permission to conduct research at Topernawi. Samples were transported to the United States for analysis under export permit M-2273-2020-2-07 from the Directorate of Mines, Republic of Kenya.

SUPPLEMENTARY MATERIAL

The Supplementary Material for this article can be found online at: https://www.frontiersin.org/articles/10.3389/feart.2022.799097/full#supplementary-material

REFERENCES

Boone, S. C., Kohn, B. P., Gleadow, A. J. W., Morley, C. K., Seiler, C., and Foster, D. A. (2019). Birth of the East African Rift System: Nucleation of Magmatism and Strain in the Turkana Depression. *Geology* 47, 886–890. doi:10.1130/g46468.1

Boone, S. C., Kohn, B. P., Gleadow, A. J. W., Morley, C. K., Seiler, C., Foster, D. A., et al. (2018). Tectono-thermal Evolution of a Long-Lived Segment of the East African Rift System: Thermochronological Insights from the North Lokichar Basin, Turkana, Kenya. *Tectonophysics* 744, 23–46. doi:10.1016/j.tecto.2018.06.010

Boschetto, H. B., Brown, F. H., and Mcdougall, I. (1992). Stratigraphy of the Lothidok Range, Northern Kenya, andK/Ar Ages of its Miocene Primates. *J. Hum. Evol.* 22, 47–71. doi:10.1016/0047-2484(92)90029-9

Brown, F. H., and Mcdougall, I. (2011). Geochronology of the Turkana Depression of Northern Kenya and Southern Ethiopia. *Evol. Anthropol.* 20, 217–227. doi:10.1002/evan.20318

Coffing, K., Feibel, C., Leakey, M., and Walker, A. (1994). Four-million-year-Old Hominids from East Lake Turkana, Kenya. *Am. J. Phys. Anthropol.* 93, 55–65. doi:10.1002/ajpa.1330930104

Cowie, P. A., Gupta, S., and Dawers, N. H. (2000). Implications of Fault Array Evolution for Synrift Depocentre Development: Insights from a Numerical Fault Growth Model. *Basin Res.* 12, 241–261. doi:10.1111/j.1365-2117.2000.00126.x

Cox, S. E., Hemming, S. R., and Tootell, D. (2020). The Isotopx NGX and ATONA Faraday Amplifiers. *Geochronology* 2, 231–243. doi:10.5194/gchron-2-231-2020

Ducrocq, S., Boisserie, J.-R., Tiercelin, J.-J., Delmer, C., Garcia, G., Kyalo, M. F., et al. (2010). New Oligocene Vertebrate Localities from Northern Kenya (Turkana basin). *J. Vertebr. Paleontol.* 30, 293–299. doi:10.1080/02724630903413065

Ebinger, C. J., Yemane, T., Harding, D. J., Tesfaye, S., Kelley, S., and Rex, D. C. (2000). Rift Deflection, Migration, and Propagation: Linkage of the Ethiopian and Eastern Rifts, Africa. *Geol. Soc. America Bull.* 112, 163–176. doi:10.1130/0016-7606(2000)112<163:rdmapl>2.0.co;2

Gurnis, M., Mitrovica, J. X., Ritsema, J., and Van Heijst, H.-J. (2000). Constraining Mantle Density Structure Using Geological Evidence of Surface Uplift Rates: The Case of the African Superplume. *Geochem. Geophys. Geosystems* 1, 35. doi:10.1029/1999gc000035

Hautot, S., Tarits, P., Whaler, K., Le Gall, B., Tiercelin, J.-J., and Le Turdu, C. (2000). Deep Structure of the Baringo Rift Basin (central Kenya) from Three-Dimensional Magnetotelluric Imaging: Implications for Rift Evolution. *J. Geophys. Res.* 105, 23493–23518. doi:10.1029/2000jb900213

Jaeger, J.-J., Chavasseau, O., Lazzari, V., Naing Soe, A., Sein, C., Le Maître, A., et al. (2019). New Eocene Primate from Myanmar Shares Dental Characters with African Eocene crown Anthropoids. *Nat. Commun.* 10, 3531. doi:10.1038/s41467-019-11295-6

Kuiper, K. F., Deino, A., Hilgen, F. J., Krijgsman, W., Renne, P. R., and Wijbrans, J. R. (2008). Synchronizing Rock Clocks of Earth History. *Science* 320, 500–504. doi:10.1126/science.1154339

Leakey, M. G., Spoor, F., Brown, F. H., Gathogo, P. N., Kiarie, C., Leakey, L. N., et al. (2001). New Hominin Genus from Eastern Africa Shows Diverse Middle Pliocene Lineages. *Nature* 410, 433–440. doi:10.1038/35068500

Lee, J.-Y., Marti, K., Severinghaus, J. P., Kawamura, K., Yoo, H.-S., Lee, J. B., et al. (2006). A Redetermination of the Isotopic Abundances of Atmospheric Ar. *Geochimica et Cosmochimica Acta* 70, 4507–4512. doi:10.1016/j.gca.2006.06.1563

Macgregor, D. (2015). History of the Development of the East African Rift System: A Series of Interpreted Maps through Time. *J. Afr. Earth Sci.* 101, 232–252. doi:10.1016/j.jafrearsci.2014.09.016

McDougall, I., and Brown, F. H. (2009). Timing of Volcanism and Evolution of the Northern Kenya Rift. *Geol. Mag.* 146, 34–47. doi:10.1017/s0016756808005347

McDougall, I., and Watkins, R. T. (2006). Geochronology of the Nabwal Hills: a Record of Earliest Magmatism in the Northern Kenyan Rift Valley. *Geol. Mag.* 143, 25–39. doi:10.1017/s0016756805001184

Min, K., Mundil, R., Renne, P. R., and Ludwig, K. R. (2000). A Test for Systematic Errors in 40Ar/39Ar Geochronology through Comparison with U/Pb Analysis of a 1.1-Ga Rhyolite. *Geochimica et Cosmochimica Acta* 64, 73–98. doi:10.1016/s0016-7037(99)00204-5

Morley, C. (1999a). "Chapter 8: Basin Evolution Trends in East Africa," in *AAPG Studies in Geology# 44* (Tulsa: The American Association of Petroleum Geologists).

Morley, C., Karanja, F., Wescott, W., Stone, D., Harper, R., Wigger, S., et al. (1999). "Chapter 2: Geology and Geophysics of the Western Turkana Basins, Kenya," in *AAPG Studies in Geology# 44* (Tulsa: The American Association of Petroleum Geologists).

Morley, C. K. (1999b). "Boundary Fault Angle, with Particular Reference to the Lokichar Fault, Turkana Region, Kenya," in *Geoscience of Rift Systems—Evolution of East Africa*. Editor C. K. Morley (Tulsa: American Association of Petroleum Geologists).

Morley, C. K. (2020). Early Syn-Rift Igneous dike Patterns, Northern Kenya Rift (Turkana, Kenya): Implications for Local and Regional Stresses, Tectonics, and Magma-Structure Interactions. *Geosphere* 16, 890–918. doi:10.1130/ges02107.1

Morley, C. K., Wescott, W. A., Stone, D. M., Harper, R. M., Wigger, S. T., and Karanja, F. M. (1992). Tectonic Evolution of the Northern Kenyan Rift. *J. Geol. Soc.* 149, 333–348. doi:10.1144/gsjgs.149.3.0333

Moucha, R., and Forte, A. M. (2011). Changes in African Topography Driven by Mantle Convection. *Nat. Geosci* 4, 707–712. doi:10.1038/ngeo1235

Muia, G. (2015). The"Turkana Grits": Potential Hydrocarbon Reservoirs of the Northern and Central Kenya Basins. *Rennes* 1, 202. Available at: https://hal-insu.archives-ouvertes.fr/tel-01379989/file/MUIA_George.pdf.

Ragon, T., Nutz, A., Schuster, M., Ghienne, J. F., Ruffet, G., Rubino, J. L., et al. (2019). Evolution of the Northern Turkana Depression (East African Rift System, Kenya) during the Cenozoic Rifting: New Insights from the Ekitale Basin (28-25.5 Ma). *Geol. J.* 54, 3468–3488. doi:10.1002/gj.3339

Renne, P. R., Swisher, C. C., Deino, A. L., Karner, D. B., Owens, T. L., and Depaolo, D. J. (1998). Intercalibration of Standards, Absolute Ages and Uncertainties in 40Ar/39Ar Dating. *Chem. Geology.* 145, 117–152. doi:10.1016/s0009-2541(97)00159-9

Roberts, E. M., Stevens, N. J., O'Connor, P. M., Dirks, P. H. G. M., Gottfried, M. D., Clyde, W. C., et al. (2012). Initiation of the Western branch of the East African Rift Coeval with the Eastern branch. *Nat. Geosci* 5, 289–294. doi:10.1038/ngeo1432

Sadler, P. M. (1981). Sediment Accumulation Rates and the Completeness of Stratigraphic Sections. *J. Geology.* 89, 569–584. doi:10.1086/628623

Sadler, P. M. (1999). The Influence of Hiatuses on Sediment Accumulation Rates. *GeoResearch Forum* 5, 15–40.

Schofield, N., Newton, R., Thackrey, S., Watson, D., Jolley, D., and Morley, C. (2021). Linking Surface and Subsurface Volcanic Stratigraphy in the Turkana Depression of the East African Rift System. *J. Geol. Soc.* 178, jgs2020–110. doi:10.1144/jgs2020-110

Sousa, F. C. S., Hemming, S., Hatton, K., Rasbury, T., Steponaitis, E., and Princehouse, P. (2020). "Geochronology and Stratigraphy of the Ekitale Basin," in American Geophysical Union, Fall Meeting 2020, Turkana County, Kenya, December 1-17, 2020.

Vetel, W., and Le Gall, B. (2006). Dynamics of Prolonged continental Extension in Magmatic Rifts: the Turkana Rift Case Study (North Kenya). *Geol. Soc. Lond. Spec. Publications* 259, 209–233. doi:10.1144/gsl.sp.2006.259.01.17

Vétel, W., Le Gall, B., and Walsh, J. J. (2005). Geometry and Growth of an Inner Rift Fault Pattern: the Kino Sogo Fault Belt, Turkana Rift (North Kenya). *J. Struct. Geology.* 27, 2204–2222. doi:10.1016/j.jsg.2005.07.003

Werdelin, L., and Sanders, W. J. (2010). *Cenozoic Mammals of Africa*. Berkeley, USA: University of California Press.

Wescott, W., Wigger, S., Stone, D., and Morley, C. (1999). "Chapter 3: Geology and Geophysics of the Lotikipi Plain," in *AAPG Studies*

in Geology# 44 (Tulsa: The American Association of Petroleum Geologists).

Conflict of Interest: The authors declare that the research was conducted in the absence of any commercial or financial relationships that could be construed as a potential conflict of interest.

Publisher's Note: All claims expressed in this article are solely those of the authors and do not necessarily represent those of their affiliated organizations, or those of the publisher, the editors and the reviewers. Any product that may be evaluated in this article, or claim that may be made by its manufacturer, is not guaranteed or endorsed by the publisher.